Carbohydrate Polymers 298 (2022) 120127

Contents lists available at ScienceDirect

Carbohydrate Polymers

journal homepage: www.elsevier.com/locate/carbpol

nHA-loaded gelatin/alginate hydrogel with combined physical and bioactive features for maxillofacial bone repair

Xiaohu Zhou [d,1], Jiwei Sun [a,b,c,1], Keqi Wo [a,b,c,1], Haojie Wei [a,b,c], Haoqi Lei [a,b,c], Junyuan Zhang [a,b,c], Xiaofeng Lu [a,b,c], Feng Mei [a,b,c], Qingming Tang [a,b,c], Yifan Wang [a,b,c], Zhiqiang Luo [e], Lihong Fan [d,*], Yingying Chu [d,*], Lili Chen [a,b,c,**]

[a] Department of Stomatology, Union Hospital, Tongji Medical College, Huazhong University of Science and Technology, Wuhan 430022, China
[b] School of Stomatology, Tongji Medical College, Huazhong University of Science and Technology, Wuhan 430030, China
[c] Hubei Province Key Laboratory of Oral and Maxillofacial Development and Regeneration, Wuhan 430022, China
[d] School of Chemistry, Chemical Engineering and Life Sciences, Wuhan University of Technology, Wuhan 430070, China
[e] National Engineering Research Center for Nanomedicine, College of Life Science and Technology, Huazhong University of Science and Technology, Wuhan 430074, China

ARTICLE INFO

Keywords:
Multi-porous surface
Interactive platform
Immunomodulation osteogenesis

ABSTRACT

Critical-sized maxillofacial bone defects have been a tough clinical challenge considering their requirements for functional and structural repair. In this study, an injectable in-situ forming double cross-linked hydrogel was prepared from gelatin (Gel), 20 mg/mL alginate dialdehyde (ADA), 4.5 mg/mL Ca^{2+} and borax. Improved properties of composite hydrogel might well fit and cover irregular geometric shape of facial bone defects, support facial structures and conduct masticatory force. We innovatively constructed a bioactive poly-porous structure by decoration with nano-sized hydroxyapatite (nHA). The highly ordered, homogeneous and size-confined porous surface served as an interactive osteogenic platform for communication and interplay between macrophages and bone marrow derived stem cells (BMSCs). Effective macrophage-BMSC crosstalk well explained the remarkable efficiency of nHA-loaded gelatin/alginate hydrogel (nHA@Gel/ADA) in the repair of critical-size skull bone defect. Collectively, the composite hydrogel constructed here might serve as a promising alternative in repair process of complex maxillofacial bone defects.

1. Introduction

Maxillofacial bone defects caused by trauma, tumor and surgery have become a major challenge for maxillofacial clinical medicine (Short et al., 2015). Complicated geometric shape, unique spatial association with facial structures and mechanical requirements for masticatory force of maxillofacial bone as well as potential postoperative complication further raise the difficulty of complete and accurate maxillofacial bone repair (Elsalanty & Genecov, 2009; Tan et al., 2021). However, poor degradability, insufficient bioactivity, and relatively low biocompatibility still hinder applications of current biosynthetic bone repairing materials (Hurle et al., 2022). Therefore, research on novel biomaterials with excellent mechanical properties and biological effects for maxillofacial bone repair is urgent and necessary.

Injectable in-situ forming hydrogels consisting of natural components, have been widely explored in bone regeneration due to their excellent biocompatibility and bioactivity. However, deficiency in physical properties restricted their application in maxillofacial bone repair (Bai et al., 2017). Thus, new strategies ought to be developed for improvement of biological and mechanical properties simultaneously.

During osteogenic process, macrophages mainly accelerate bone tissue regeneration by modulating biological functions through paracrine pathway (Zhu et al., 2021). Meanwhile, bone marrow stem cells (BMSCs) are vital during osteogenic phase due to their self-replication and osteogenic differentiation (Graham et al., 2016). Current bioactive hydrogels mainly drive bone healing by either directly controlling the

* Corresponding authors at: School of Chemistry, Chemical Engineering and Life Sciences, Wuhan University of Technology, Wuhan 430070, China.
** Correspondence to: L. Chen, Department of Stomatology, Union Hospital, Tongji Medical College, Huazhong University of Science and Technology, 1277 Jiefang Avenue, Wuhan 430022, China.
E-mail addresses: Fanlihong2000@163.com (L. Fan), y.chu@whut.edu.cn (Y. Chu), chenlili1030@hust.edu.cn (L. Chen).
[1] Xiaohu Zhou, Jiwei Sun and Keqi Wo contributed equally to this article.

https://doi.org/10.1016/j.carbpol.2022.120127
Received 18 July 2022; Received in revised form 5 September 2022; Accepted 14 September 2022
Available online 17 September 2022

polarization of macrophages or promoting osteogenic differentiation of BMSCs. However, deficiency in dual modulatory potential and lack in the control of communication between macrophages and BMSCs further compromise the success of current bioactive materials in bone regeneration (Sylwia, Anna, Miroslaw, & Barbara, 2020). Nano hydroxyapatite (nHA) is the main inorganic component of bone tissue, exhibiting the potential to promote osteogenic differentiation of BMSCs. However, its lack in mechanical stability and tissue adhesion restricts its stability at the defect sites.

In this study, we developed a novel gelatin-based composite hydrogel system double cross-linked by ADA (covalent crosslinking) and Ca^{2+} (ion crosslinking) to acquire predominantly enhanced tensile and compressive strength, self-healing potential and shape adaptability. Meanwhile, borax was introduced into this system to accelerate the gelation process as well as to construct multiple networks via ionic crosslinking. By addition of degradable polyethylene glycol (PEG), an excellent stability of chemical bonds inside the system was successfully acquired. nHA was then evenly distributed into the hydrogel system for construction of an osteogenic platform regulating interplay between macrophages and BMSCs. By decoration of nHA, the hydrogel system was expected to self-assemble into a highly ordered porous structure. Specifically, the pore size of the composite hydrogel was roughly 10–30 μm, which is consistent with the diameter of cells inside osteogenic microenvironment (Krombach et al., 1997; Samsonraj et al., 2017). Taking these advantages, nHA decorated Gel-ADA hydrogel was expected to act as an interactive platform regulating the mutual communication between macrophages and BMSCs for bone regeneration. Thereby, the newly constructed composite hydrogel as a novel osteogenic platform is promising in functional and regenerative repair of maxillofacial bone.

2. Experimental section

2.1. Materials

Sodium alginate (SA, AR, Mw: 20,000–32,000, M/G: 1.61 ± 0.02, algea-derived) and gelatin (Gel, AR) were purchased from Aladdin Reagent (Shanghai) Co., Ltd.; hydroxylamine hydrochloride (AR, 98.5 %) was purchased from Maclean's Reagent Co.; sodium periodate ($NaIO_4$), anhydrous ethanol (EtOH), sodium tetraborate decahydrate (borax, $Na_2B_4O_7$-$10H_2O$), calcium chloride ($CaCl_2$), sodium hydroxide (NaOH), polyethylene glycol (PEG, 2000), nanohydroxyapatite (nHA, 200 nm), phosphate buffer (PBS, pH = 7.4) were purchased from Sinopharm Chemical Reagent Co., Ltd. and were analytically pure. Rat bone marrow mesenchymal stem cells (rBMSCs) were obtained from the bone marrow of 4-week-old male Sprague Dawley (SD) rats and maintained in Minimum Essential Medium Alpha (1×) (α-MEM) containing 10 % fetal bovine serum (FBS). Passage 4 (P4) rBMSCs were used for the following experiments. THP-1 cells were obtained from American Type Culture Collection (ATCC) and maintained in 1640 medium containing 10 % FBS. Human bone marrow mesenchymal stem cells (h-BMSCs) were obtained from the Orthopedic Laboratory of Wuhan Union Hospital and maintained in Minimum Essential Medium Alpha (1×) (α-MEM) containing 10 % FBS. Passage 4 (P4) h-BMSCs were used for the following experiments. THP-1 cell lines within 30 passages were used for the following experiments. All cells were cultured within a humidified incubator at 37 °C with 5 % CO_2.

2.2. Preparation of sodium di-formaldehyde-alginate (ADA)

According to previous reports, di-formalized sodium alginate (ADA) was prepared from the oxidation of sodium alginate in the presence of sodium periodate (Wang et al., 2022). Typically, 20 g sodium alginate was evenly dispersed in 100 mL of anhydrous ethanol solution, followed by the addition of 10.8 g of sodium periodate which was dissolved in 100 mL deionized water. The reaction mixture was stirred at room temperature and kept in dark for 6 h. Afterwards, the reaction mixture was dialyzed with deionized water (2.5 L) and the water was changed every 6 h until unreacted periodate was eliminated, which was indicated by the absence of precipitation when 0.5 mL dialysate was withdraw and then added to 0.5 mL 1 % silver nitrate solution. The dialysate was concentrated by rotatory evaporation and then freeze-dried to obtain pure ADA. Finally, the oxidation degree of ADA was evaluated by titration of hydroxylamine hydrochloride, which was 43 % (Emami, Ehsani, Zandi, & Foudazi, 2018).

2.3. Preparation of composite hydrogels

At room temperature, 4 % (w:v) ADA and 2 % (w:v) borax were dissolved in different mass fractions of PEG 2000 solution, noted as liquid A. Similarly, 12 % (w:v) gelatin was dissolved in different mass fractions of PEG 2000 solution at 37 °C, noted as liquid B. ADA-Gel hydrogels (AG) were homogeneously mixed by A:B = 1:1 (v:v) and left to stand at 37 °C. And ADA-Gel/Ca^{2+} hydrogel (CaAG) was made by adding a certain amount of $CaCl_2$ solution to the AG precursor solution and left to stand at 37 °C. Similarly, a certain amount of nHA (10 %, 20 %, 30 %, w/w) at the concentration of 9 mg/mL, 18 mg/mL and 27 mg/mL respectively was added to the CaAG precursor solution and then homogeneously mixed and left to obtain the hydrogel HA-X (X stands for 10, 20 and 30, respectively, which refers to the mass fraction of loaded nHA). The nHA@Gel/ADA hydrogels were prepared as shown in Table S1.

2.4. Material characterization

Fourier transform infrared spectroscopy (FTIR, Nicoet 170SX, USA): FTIR of SA, ADA, AG, CaAG and HA-X was measured by the KBr-disk method. Specifically, the test samples were freeze-dried and mixed with potassium bromide powder, then the mixture was finely ground and pressed into thin slices. The spectra were scanned in the range of 400–4000 cm^{-1}.

Scanning electron microscopy (SEM): 1 mL of each hydrogel samples were kept in a freezer at −80 °C for 12 h and then freeze-dried. The freeze-dried samples were then placed in liquid nitrogen for brittle fracture and the cross-sections were coated with gold. The internal microstructure of the hydrogels was observed under a scanning electron microscope (SEM, S-4800, Hitachi, Japan).

2.5. Rheological studies

Rheological properties of the prepared hydrogel samples were tested by Discovery HR-2 rheometer (TA Instruments, USA) with a 40 mm plate and 2.0 mm gap. Typically, hydrogel samples were equilibrated at 4 °C for 6 h prior to test to reach complete and uniform gelation. (1) Oscillatory frequency scan measurements were carried out at 10 % strain with an angular frequency range of 0.1 to 100 rad/s to determine the energy storage modulus (G′) and loss modulus (G″) of the hydrogel at 37 °C. (2) The strain amplitude sweep test (γ = 1– 5000 %) was performed to detect the critical strain point of hydrogels at 37 °C. (3) The alternate step strain sweep test at 37 °C was performed at an oscillation frequency (10 rad/s). Amplitude oscillatory strains were switched from small strain (γ = 10 %) to subsequent large strain (γ = 3000 %) with 200 s for every strain interval. (4) Besides, the viscosity measurements as a function of shear rate (0– 100 s − 1) at 37 °C.

2.6. Mechanical performance tests

2.6.1. Tensile property test

The hydrogel sample was cast into dumbbell type (75 × 4 mm) and balanced for 6 h. Afterwards, they were stretched at a rate of 20 mm/min by using a universal tester with 200 N weighing sensor (CMT6503, USA) at room temperature until they broke and record the maximum

tensile strength. The toughness was calculated by integrating the area underneath the stress-strain curve of the hydrogel sample (Chen et al., 2022). The formed hydrogels were cut in equal parts from the middle and glued together, and after 2 h, the self-healing ability of the hydrogels was characterized by the above-mentioned stretching method.

2.7. Indirect BMSC/macrophage co-culture

h-BMSCs were cultured on the hydrogel for 3 days and then the supernatant was extracted and mixed with 1640 medium. THP-1 cells were cultured in above liquid added Phorbol 12-myristate 13-acetate (PMA) at a concentration of 100 ng/mL. Similarly, THP-1 cells were cultured on the hydrogel for 3 days and the supernatant was extracted and mixed with osteogenic differentiation medium for culturing BMSCs.

2.8. Alkaline phosphatase assay

The BMSCs were fixed with 4 % paraformaldehyde solution (PFA) and incubated in osteogenic differentiation medium for 7 days. Afterwards, the BCIP/NBT Alkaline Phosphatase Color Development Kit (Beyotime Biotechnology, China, C3206) was conducted according to the instructions.

2.9. Quantitative real-time PCR (RT-qPCR)

Total RNA extraction of cells was performed using Trizol reagent (Takara, Japan) according to the manufacturer's protocol. Complementary DNA was generated using PrimeScript RT Reagent Kit (Takara). Subsequent Fast SYBR Green qPCR were performed on Step One Plus RT-PCR systems (Applied Biosystems). Experiments were performed at least three times, after which the relative quantification of target genes were normalized to GAPDH control and calculated using $2^{-\Delta\Delta Ct}$ method. Primers were listed in Table S2.

2.10. Immunofluorescence

Cells were seeded and cultured on sterile glass cover slips in 12-well plates. When cell density reaches to 50 %, they were fixed with 4 % PFA f or 15 min, permeabilizated with 0.5 % Triton X-100 and then blocked with 5 % bovine serum albumin. After that, cells were stained with primary antibodies COL1A1 (ABclonal, A1352, 1:200), OPG (abcam, ab183910, 1:200), RUNX2 (abcam, ab192256, 1:200), CD206 (Proteintech, 60143-1-Ig, 1:200) overnight at 4 °C. Later, cells were incubated with Coralite488-conjugated Goat Anti-Rabbit IgG (H + L) secondary antibody (1:200) and Cy3-conjugated Affinipure Goat Anti-Mouse IgG (H + L) secondary antibody (1:200) for 1 h at room temperature, DAPI was used for nuclear counterstaining. Fluorescent images were acquired on a confocal microscope (Nikon A1-Si) with NIS software for collection.

2.11. Animal study

All animal procedures were carried out in line with the ARRIVE guidelines and in accordance with National Research Council's Guide for the Care and Use of Laboratory Animals as well as Institutional Animal Care and Use Committee of Tongji Medical College (Wuhan, China) and experiments were approved by the Animal Ethics Committee of Tongji Medical College (Wuhan, China). The bone defects were created on the bilateral skull of male Sprague Dawley (SD) rats at the age of 6–8 weeks (weight: 390–410 g). All rats were divided in to three groups ($n = 5$ per group): (1) AG, (2) CaAG, and (3) HA-30. After anesthetization and disinfection. Circular defects were made by means of a 5 mm diameter trephine. After 6 weeks, the rats were sacrificed and the skulls were collected for further experiments.

2.12. Micro-CT analysis

New bone formation was screened by Radiological monitoring. After fixed in 4 % PFA for 24 h, the skull specimens were scanned by Skyscan 1076 micro-CT (Inveon Multimodality Scanner; Siemens, Erlangen, Germany) and three-dimensional images of the skull specimens were reconstructed from the scans by the micro-CT system software package. The images of each group were measured to calculate the new bone volume ratio (bone volume to total volume, BV/TV), trabecular numbers (Trabecular Number, Tb. N) to assess new bone formation circumstance.

2.13. Statistical analysis

All data were analyzed using one-way ANOVA by GraphPad Prism 8.0. Data were expressed as mean ± standard deviation and statistical significance was accepted at $^{*}p < 0.05$, $^{**}p < 0.01$.

3. Results and discussion

3.1. Preparation and characterization of nHA@Gel/ADA hydrogels

To construct composite hydrogels, alginate and gelatin were first mixed and cross-linked by imine linkage (precursor AG), followed by the addition of Ca^{2+} for further ionic linking to prepare hydrogel CaAG (Fig. 1A). After nHA was identified by SEM and EDS tests (Fig. S1), it was then dopped into the composite system to endow the composite hydrogel with improved mechanical properties and biological activities. Along with increasing addition of Ca^{2+} and nHA, the gel formation time and quality showed an increasing tendency (Table S2). Notably, to furthermore improve the thermal stability of the composite hydrogel, 5 % (w/v) PEG 2000 solution was utilized to dissolve each raw material in preparation process. Successful preparation of the precursors and hydrogels was confirmed by Fourier Transform infrared spectroscopy (FTIR) (Fig. 1B). Specifically, the structure of ADA was verified by the appearance of new peaks at 2853 cm^{-1} and 1748 cm^{-1}, which were attributed to C—H and C═O stretching vibrations on the aldehyde groups in ADA (Jejurikar et al., 2012). Afterwards, the formation of Schiff base between gelatins and ADA to prepare precursor AG was confirmed by the occurrence of new peak at 1566 cm^{-1} in AG's spectrum, which was attributed to stretching vibration of amine bond (C═N) (Ding, Zhou, Zeng, Wang, & Shi, 2017). The amplitude of 1643 cm^{-1} absorption peak vibration and the significant change of peak in the range 1200–1600 cm^{-1} in CaAG spectrum when compared to AG were attributed to the interaction between Ca^{2+} and the carboxyl group (–COOH) in AG (Ma, E, & Yang, 2021). Finally, successful doping of nHA into CaAG to produce hydrogel HA-X was verified as a new peak occurred at 1140 cm^{-1} in HA-30 spectrum, which was attributed to the stretching vibration of the phosphorus-oxygen double bond (P═O) in nHA (Barros et al., 2019). By introduction of 5 % PEG, the composite hydrogels acquired the lowest degradation rate <50 % within 10 days at natural environment (Fig. S3). To test the stability of hydrogels in acidic and alkaline environment, we performed degradation tests on composite hydrogels under different pH conditions. No remarkable changes of degradation were observed within 6 days among three groups due to introduction of 5 % PEG to form compact hydrogel network. Furthermore, either in acidic (pH = 5.5) or alkaline (pH = 9.5) environment, composite hydrogels all displayed an accelerated degradation process, with the degradation rate increasing about 10 %–15 % at day 10 (Fig. S4). This might be explained by the destruction of Schiff bases and alginate-Ca^{2+} ionic linking by acidic and alkaline influence (Huang, Mu, Zhao, Han, & Guo, 2022).

Excellent three-dimensional structures of the prepared hydrogels were revealed by scanning electron microscopy (SEM) (Fig. 1C–D, Fig. S2). Large pore size (70 μm) and smooth micro porous surfaces were observed in AG hydrogel while that of CaAG turned into a dense wrinkled structure due to the formation of ionic bonds between alginate and

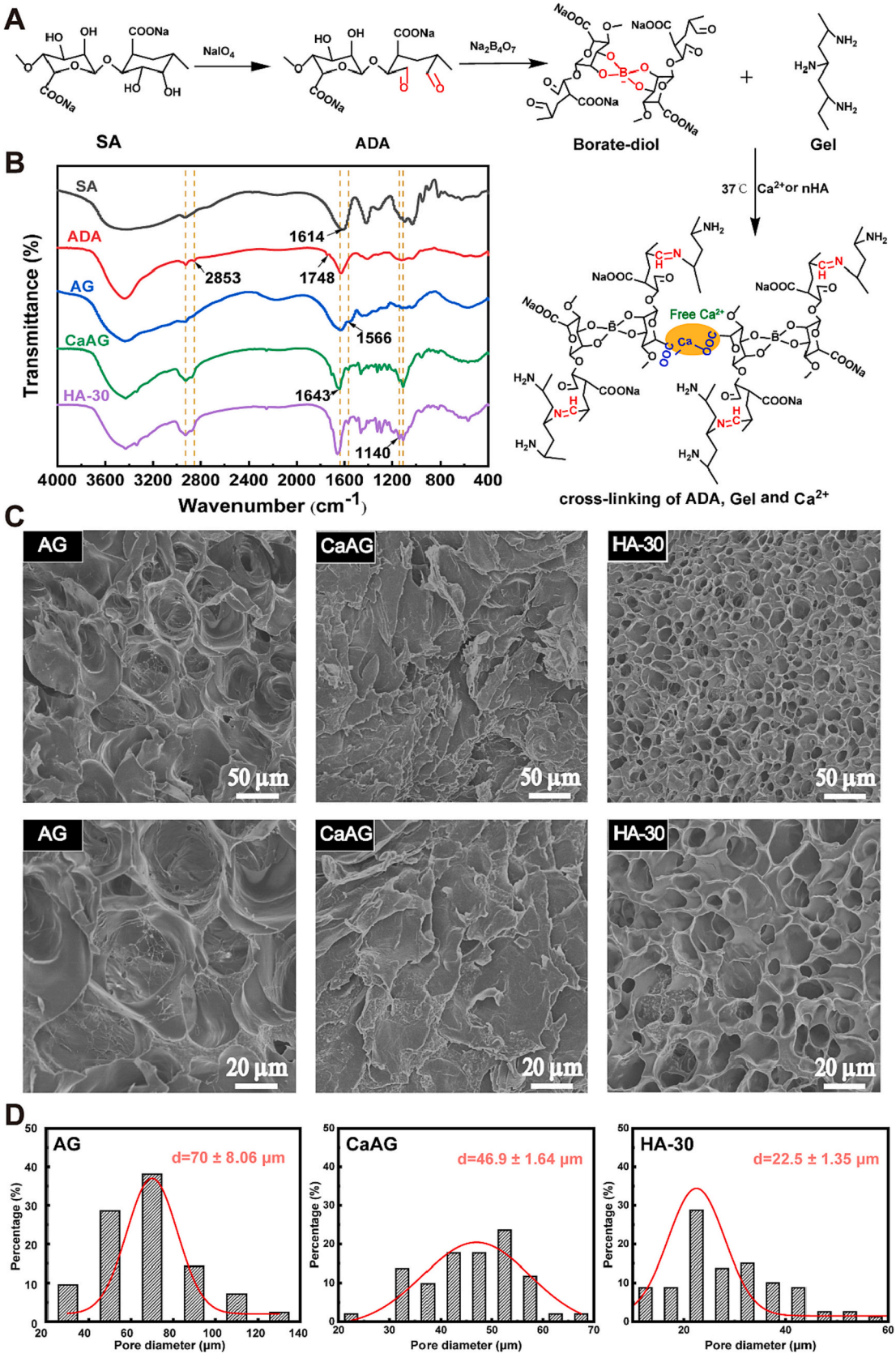

Fig. 1. Preparation and characterization of nHA@Gel/ADA.
A) Synthetic procedures of composite hydrogels. B) FTIR spectrum of SA, ADA, AG, CaAG and HA-30. C) SEM images display crossing sections of AG, CaAG and HA-30 (scale bars = 50 μm and 20 μm). D) Pore size distribution of AG, CaAG and HA-30.

Ca^{2+} to produce an "egg box" structure. Afterwards, the dense wrinkled structure gradually transferred into porous structure upon addition of nHA, among which hydrogels dopped with 30 % nHA exhibited smallest pore size (15 μm) with most uniform pore distribution. We hypothesized that PO_4^{3-}, Ca^{2+} ions and the –OH groups in nHA might interact with –NH groups in crosslinked polymer chains, leading to additional ionic cross-linking between ADA, Gel, Ca^{2+} and nHA. Therefore, the addition of nHA might restricts the mobility of the polymer chains, thus resulting in a more compact and restricted hydrogel lattice (Hassani, Khoshfetrat, Rahbarghazi, & Sakai, 2022). Previous studies revealed that pore size of the matrix could influence cellular behaviors, such as cell migration rate and cell proliferation rate (Evans, Oreffo, Healy, Thurner, & Man, 2013), and this could be explained by surface tensile and mechanical stimulus induced by different pore sizes (Rumpler, Woesz, Dunlop, van Dongen, & Fratzl, 2008). The sizes of cells inside regenerative microenvironment ranges from 10 μm to 30 μm (Lloyd, 2013; Mueller, 2015), which just matched up with surface porous structures of HA-30. In addition, porous biomaterials with diameters about 10 μm–20 μm exhibited promising effect on secretory potential, cell adhesion and differentiation(Zheng et al., 2020). Thus, it is speculated that the construction of porous platform via introduction of 30 % nHA might possess some potential biological functions for regulation of cell behavior during bone regeneration. Swelling rate of CaAG and AG showed a significant difference, which might be due to the increased cross-link density within the hydrogel upon the addition of Ca^{2+}, which leads to decreased water absorption ability, thus resulting in decreased swelling rate. However, the swelling rate and water retention property of HA-30 showed no significant difference with CaAG, suggesting that the addition of proper amount of nHA into the composite system would not destroy the inherent properties of ADA-Gel hydrogels (Fig. S5–S6). Altogether, we successfully constructed nHA@Gel/ADA hydrogels (HA-X), with a highly ordered porous structure and suitable porous size, which might provide a microenvironment favorable for bone regeneration via regulating the cellular behaviors by both chemical composition and spatial

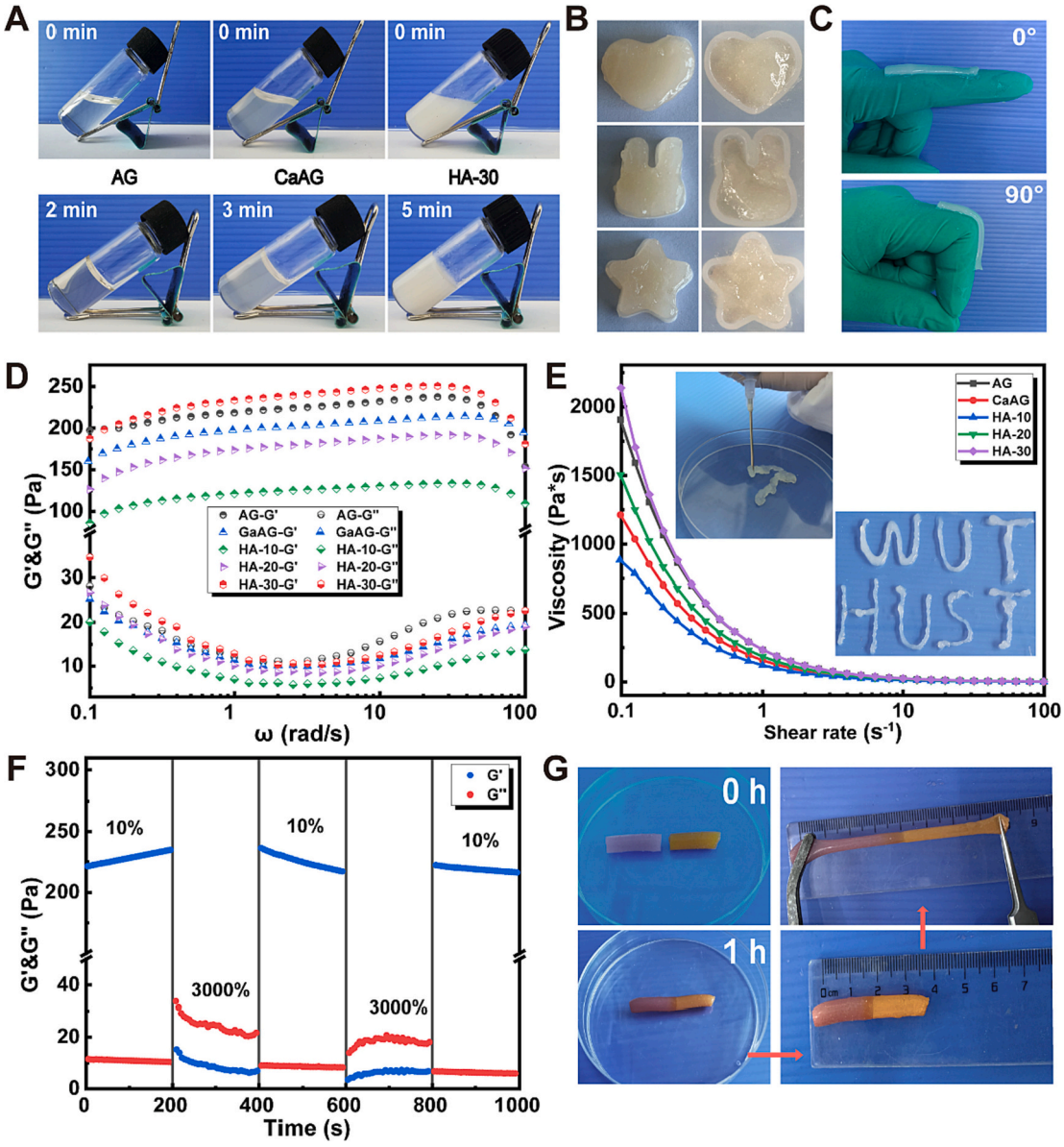

Fig. 2. Physicochemical properties of nHA@Gel/ADA.
A) Appearance of prepared composite hydrogels before and after gelation. B) Adaptability of HA-30 in molds with different shapes. C) Flexibility of HA-30 adhered on knuckles. D) Viscoelastic behavior of composite hydrogels. E) Thinning shear behavior of composite hydrogels at 37 °C, and photos of injectable objects (HA-30 as an example). F) Alternate strain sweep of HA-30 at 37 °C. G) Photographs of macroscopic self-healing properties of HA-30.

structure.

3.2. Physicochemical properties of nHA@Gel/ADA hydrogels

Physicochemical properties of composite hydrogels were then performed to assess their applicability in maxillofacial bone repair. Both of AG, CaAG and HA-30 hydrogels underwent rapid gelation (within 5 min) at 37 °C due to the formation of dynamic Schiff base and ion crosslinking in the hydrogel system (Fig. 2A). As irregularity is an important feature of maxillofacial bone defects caused by trauma, tumor resection and periodontitis, the shape adaptability of composite hydrogels was also evaluated. nHA@Gel/ADA hydrogels could adapt to the mold shape within 10 min and remain this moldability performance after removing it from the molds (Fig. 2B). Additionally, the hydrogel could adhere on the knuckle for 90° bending without dislodging and deformation (Fig. 2C), suggesting the capacity of the hydrogel to adapt to various forms of bone defects.

Superior viscoelastic behavior and injectability of the composite hydrogels were demonstrated via rheological studies (Fig. 2D). Specifically, the energy storage modulus (G′) value was consistently higher than the loss modulus (G″) value within the range of tested frequencies, indicating that all hydrogels possess internal three-dimensional networks with favorable elastic properties. Meanwhile, both of the G′ and G″ value of composite hydrogels were correlated with angular frequency due to the dynamic cross-linking bonds in hydrogel network as slight changes were observed upon the variation of angular frequency. Notably, the G′ and G″ value of HA-30 were higher than other samples under the tested frequencies, suggesting that the addition of 30 % nHA particles could improve the viscoelastic behavior of the hydrogel, which was in accordance with the highest viscosity possessed by HA-30 (Fig. 2E). Injectability of prepared hydrogels was also verified as alphabets were typed via syringe filled with HA-30 hydrogel. Afterwards, dynamic strain scanning tests (Fig. S7) were conducted to determine the critical sheer strain of HA-30 (2400 %) for further investigation on its self-healing ability. When the strain applied to the composite hydrogel is greater than this critical value, the internal network structure of the hydrogel will collapse, and the solid hydrogel will transform into a fluid state due to the breakage of the imine bonds within the hydrogel. Therefore, the self-healing ability of HA-30 was assessed under successive alternating strain values of 10 % and 3000 % (Fig. 2F). When large strain was stopped and a small strain (10 %) was applied, the G′ and G″ value of HA-30 almost recovered to their initial state within few seconds, which was attributed to the reversible nature of the imine and ionic bonds, thus allowing for the rapid reconstruction of the broken bonds. More importantly, such recovery was reproducible, suggesting the excellent self-healing capability of HA-30. Accordingly, superior self-healing ability of the hydrogels was also evidenced by the recovery of faulted hydrogel within 1 h with retained tensile property (Fig. 2G, Fig. S9A). We then performed the tensile test of hydrogels after self-healing, and results showed that the HA-30 group remained the best tensile properties compared with other groups, the same with the tendency before self-healing (Fig. S9B, C), suggesting that this hydrogel is capable of healing itself after being ruptured by a substantial external force and maintain its therapeutic effect during bone regeneration process. Taken together, the above results validated that HA-30 possessed excellent shape adaptability, viscoelasticity, injectability and self-healing ability, all of which are beneficial for the repair of complex maxillofacial bone defects.

3.3. Mechanical properties of nHA@Gel/ADA hydrogels

As facial bone tissues are in complex anatomic structure, biomaterials applied here face the challenges of being detached and falling off from repaired tissues. Hence, adhesion property is vital for bone regeneration materials and adhesion property of HA-30 was evaluated against various surfaces, including plastics, glass, rubber, wood and bone (Fig. 3A). The adhesion strength between prepared hydrogels and porcine skin was further evaluated through lap shear tensile test (Fig. 3B–C). Specifically, the adhesion strength of CaAG (53.19 kPa) increased significantly when compared to AG (29.69 kPa), demonstrating that the formation of ionic cross-linking between Ca^{2+} and the -COOH groups in alginate could improve the structure stability and cohesion of the hydrogel, thus leading to enhanced adhesion property. A decrease in adhesive strength was observed upon the addition of nHA (the adhesive strength varied from 20 to 25 kPa), which we hypothesized that the hydrogen bond between the hydrogel and nHA could diminish the hydrogen bond between hydrogel interface and the tissue. Fortunately, the adhesive strength of HA-X was still acceptable since it is >10 kPa, which meet the requirement of injectable bone regeneration materials in long-term therapeutic process (Hongbo, Min, Yajie, Jingbo, & Renjun, 2020).

As facial bone tissues take the responsibility of supporting functional mechanical force including mastication, swallowing and language speaking, hydrogels as bone healing materials should ideally possess adequate mechanical strength and toughness. Compression experiments were performed to quantify the mechanical properties of the hydrogels. All compressive stress strain curves display a typical “J” shape, indicating that the hydrogels have a certain degree of elasticity which are similar to biological tissue (Fig. 3D) (Yinghua, Elizabeth, Stevin, & Michael, 2013). Specifically, the compressive strength of AG and CaAG at maximum strain are approximately 0.41 MPa and 0.76 MPa, suggesting that the addition of Ca^{2+} could increase the compressive resistance of hydrogel. Notably, the compressive strength of composite hydrogels further raised upon the addition of nHA due to the increased hydrogen bond formation, among which HA-30 exhibited highest compressive strength (1.52 MPa). Furthermore, the compressive modulus of AG, CaAG and HA-30 at 5–15 % strain exhibited the same trend, of which were 19.6 kPa, 63.7 kPa, and 124 kPa respectively (Fig. 3E). Tensile tests were then conducted on prepared hydrogels (Fig. 3F and Fig. S9B,S9C) and results showed that HA-30 possessed the greatest fracture stress (480 kPa at 380 % strain) when compared to AG (93 kPa at 280 % strain) and CaAG (190 kPa at 290 % strain). We subsequently tested the toughness of composite hydrogels, and results showed that the HA-30 group displayed a superior behavior in toughness property, with a 2–3 folds upregulation compared with those in other groups (Fig. 3G). By introduction of nHA into composite hydrogels, the mineral induction efficiency of composite hydrogels was also remarkably enhanced (Fig. S10). These results further proved that the addition of Ca^{2+} to form ionic-crosslinking within the hydrogel as well as further stabilization of the hydrogel structure upon the decoration of nHA could dramatically improve the mechanical properties of the composite hydrogels, which is vital for the design and preparation of biomaterials to satisfy the mechanical requirements of maxillofacial bone repair.

3.4. Biocompatibility of composite nHA@ADA-Gel hydrogels

To evaluate the biocompatibility of composite hydrogels, Cell Counting Kit 8 (CCK-8) assay was performed on macrophages and BMSCs seeded on composite hydrogels after 1, 3 and 5 days. Results showed no significant difference in cell viability among different groups (Fig. S11). Similarly, the live/dead assay suggested most of the cells within AG, CaAG and HA-30 hydrogels were kept alive after 3 days (Fig. S12). While gelatin and algin are natural extracts which are safe for biological application (Li et al., 2021), excessive addition of Ca^{2+} might produce unnecessary cytotoxicity (Giovanna et al., 2020; Yin, Hongbing, Chunlian, Chengfeng, & Xue, 2014). Thus, composite hydrogels with different concentrations of Ca^{2+} have been produced to test their influence on cell growth and viability. Results indicated that a proper range of concentrations of Ca^{2+} caused no negative effect on cell growth and viability (Fig. S13). This conclusion supported our application of Ca^{2+} at the concentration of 4.5 mg/mL in hydrogels for further

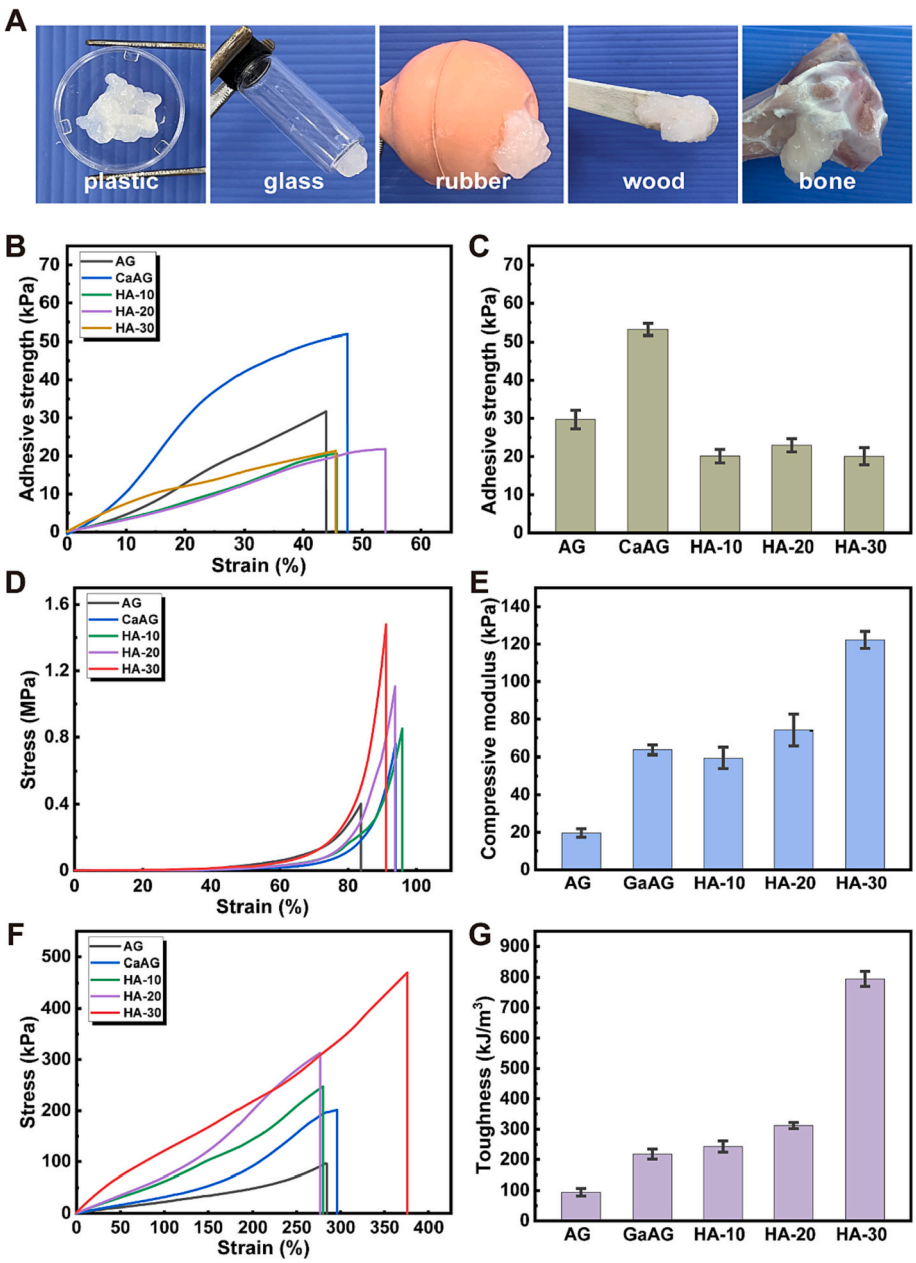

Fig. 3. Mechanical properties of nHA@Gel/ADA. A) Photographs of HA-30 adhesion to plastic, glass, rubber, wood and bone. B) Stress-strain curve of composite hydrogel adhering to fresh pigskin. C) Maximum adhesion strength of composite hydrogel adhering to fresh pigskin. D) Compressive stress-strain curves of composite hydrogels. E) Compressive modulus at 5–15 % strain of composite hydrogels. F) Tensile stress-strain curves of composite hydrogels. G) of Toughness of composite hydrogels.

functional experiments. These results indicated that the addition and proportion of fillers in composite hydrogels were appropriate, and the newly constructed composite hydrogel in our study is promising in bioengineering.

3.5. *nHA@ADA-Gel directly and indirectly drives anti-inflammatory M2 macrophage polarization*

To explore whether and how nHA@ADA-Gel hydrogels drive macrophage M2 polarization, we detected the expression of established M2 macrophage-related markers under two different conditions. In the first case, M0 macrophages were directly seeded onto hydrogel surface (Fig. 4A). Immunofluorescence assay showed that HA-30 significantly upregulated the expression of M2-associated membrane marker CD206 by >3-fold compared to that in AG and CaAG group (Fig. 4B–C) ($p < 0.0001$). Meanwhile, real-time polymerase chain reaction (RT-qPCR) study revealed that HA-30 significantly increased the expression of M2-related genes *IL12A* ($p < 0.0001$), *TGFβ* ($p < 0.01$), and *CCL2* ($p < 0.01$) (Fig. 4D–F). In the second situation, the supernatant from h-BMSCs inoculated on hydrogels was extracted and then added into the culturing medium of M0 macrophages for indirect induction of macrophage polarization (Fig. 4G). HA-30 mediated supernatant from h-BMSCs significantly upregulated membrane expression of CD206 (Fig. 4H–I) ($p < 0.01$), which was further confirmed by measuring mRNA levels of *CCR2* ($p < 0.01$), *TGFβ* ($p < 0.05$) and *CCR5* ($p < 0.05$) (Fig. 4J–L). These data suggested that HA-30 could induce polarization of M2-like macrophages either by direct effect of HA-30 itself or through indirect impact of BMSCs on HA-30. We speculated that the direct immunomodulatory function of HA-30 on macrophages could be partially attributed to the evenly distributed nHA in the hydrogel system. By secretion of chemokines such as CCL2 and CCL4, MSCs indirectly induce recruitment of macrophages into regenerative sites (Chen, Tredget, Wu, & Wu, 2008). Meanwhile, BMSCs perform immunomodulatory functions for phenotype transfer of M2-like macrophages through iNOS and COX2 dependent signaling pathway (Maggini et al., 2010). Considering multiple cellular behaviors, especially cytokine secretion and

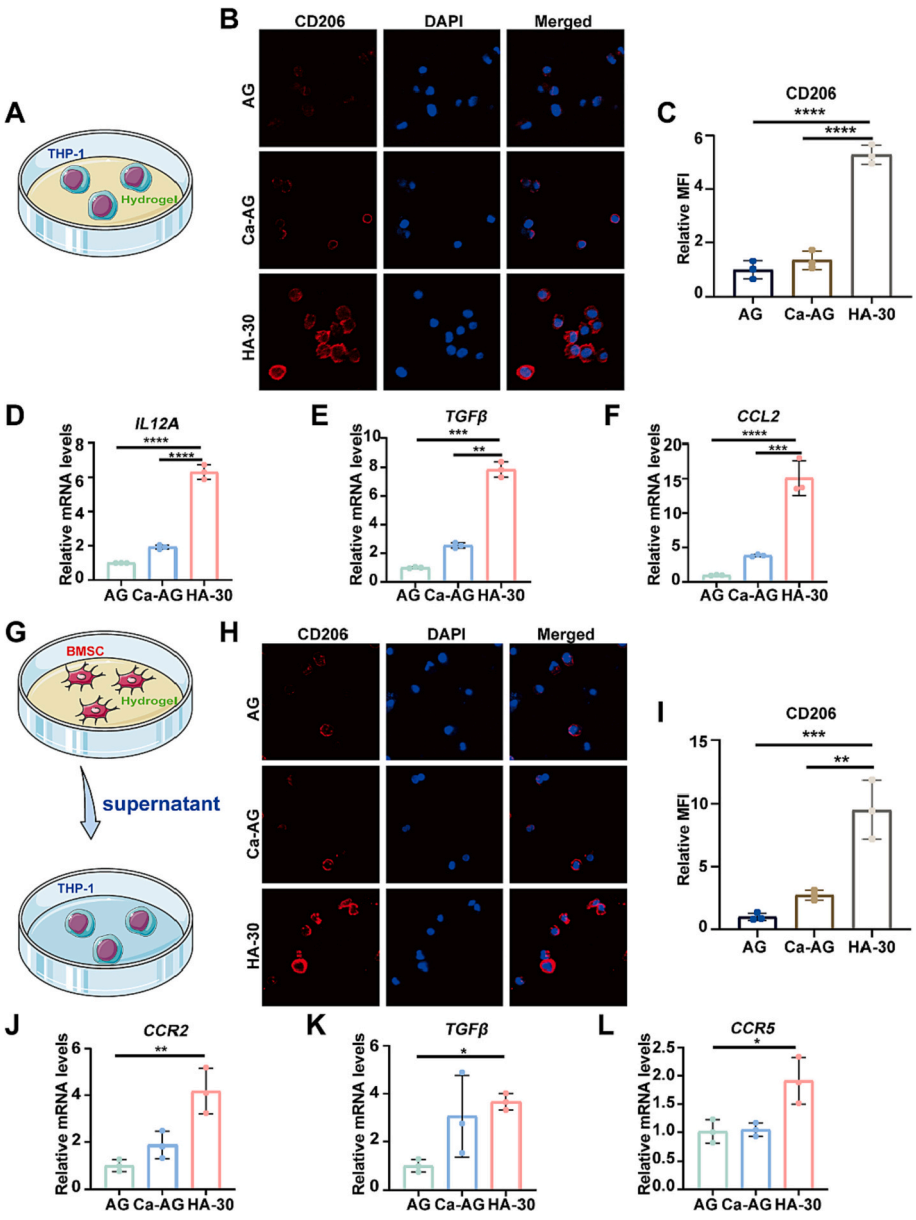

Fig. 4. nHA@Gel/ADA directly and indirectly induces macrophage anti-inflammatory differentiation. A) Schematic illustration of the process that composite hydrogels directly induced macrophage anti-inflammatory differentiation. B) Confocal microscopy images of immunofluorescence staining with CD206 (red) in THP-1 cells directly cultured on hydrogels (scale bar = 10 μm). C) Relative mean fluorescence intensity of CD206 in THP-1 cells directly cultured on hydrogels. D, E and F) RT-qPCR results of relative *IL12A*, *TGFβ* and *CCL2* mRNA expression levels in THP-1 cells directly cultured on hydrogels. G) Schematic illustration of the process that h-BMSCs cultured on hydrogels indirectly induce macrophage anti-inflammatory differentiation. H) Confocal microscopy images of immunofluorescence staining with CD206 in THP-1 cells indirectly induced by h-BMSCs cultured on hydrogels (scale bar = 10 μm). I) Relative mean fluorescence intensity of CD206 in THP-1 cells indirectly induced by h-BMSCs cultured on hydrogels. J, K and L) RT-qPCR results of relative *CCR2*, *TGFβ* and *CCR5* mRNA expressions in THP-1 cells indirectly induced by h-BMSCs cultured on hydrogels. $^{*}p < 0.05$, $^{**}p < 0.01$, $^{***}p < 0.001$, $^{****}p < 0.0001$.

immunomodulation, are associated with surface morphology of biomaterials(Jin et al., 2019), the special appearance of nHA@ADA-Gel hydrogels denoted by uniformly distributed poles with their sizes matched to cell diameters might steer the direct and indirect M2 polarization.

3.6. Polarized M2 macrophages on nHA@ADA-Gel promote osteogenic differentiation of BMSCs

We next attempted to determine the impact of hydrogel-derived M2 macrophages on BMSC osteogenic differentiation. Supernatants of differentiated M2 macrophages on hydrogels were collected for stimulation of BMSCs (Fig. 5A). Human BMSCs exhibit comparatively higher levels of alkaline phosphatase (ALP) levels when compared to those of the other two groups (Fig. 5B). Immunofluorescence staining for two major osteogenesis-related markers, type I collagen (COL1) ($p < 0.05$) and Runt-related Transcription Factor 2 (RUNX2) ($p < 0.01$) further validated these findings (Fig. 5C–F). Meanwhile, the mRNA levels of classical osteogenic-related genes, including *OSX* ($p < 0.05$), *RUNX2* ($p < 0.05$), *OPN* and *COL1* ($p < 0.01$), were all statistically upregulated under both 7 days and 14 days osteogenic induction (Fig. 5G–J, Fig. S16). These findings indicated that polarized macrophages directly induced by HA-30 can enhance BMSCs osteogenic differentiation in return. Next, role of polarized macrophages indirectly driven by BMSCs on osteogenesis were assayed (Fig. S15A). Accordingly, immunofluorescent staining validated the highest expression levels of RUNX2 and OPG in HA-30 group (Fig. S15B–E). Statistical analysis of mRNA expression of *COL1* ($p < 0.01$), *OPN* ($p < 0.05$), and *RUNX2* further demonstrated that indirectly polarized macrophages in HA-30 could significantly promote osteogenic differentiation (Fig. S8F-S8H). According to previous literatures, polarized M2 macrophages contribute to recruitment of BMSCs and osteoprogenitors to defect regions via CCL2, CXCL8 and SDF-1 (Belema-Bedada, Uchida, Martire, Kostin, & Braun, 2008), and promote MSC-mediated bone formation process and enhanced matrix mineralization by secretion of signaling factors (Murray & Wynn, 2011). Taken together, the composite hydrogel acts as an interactive platform for efficient crosstalk between macrophages and BMSCs. The pro-polarization effect from BMSCs and pro-osteogenesis role of macrophages on nHA@ADA-Gel work together to form a positive feedback loop, leading to accelerated bone regeneration process.

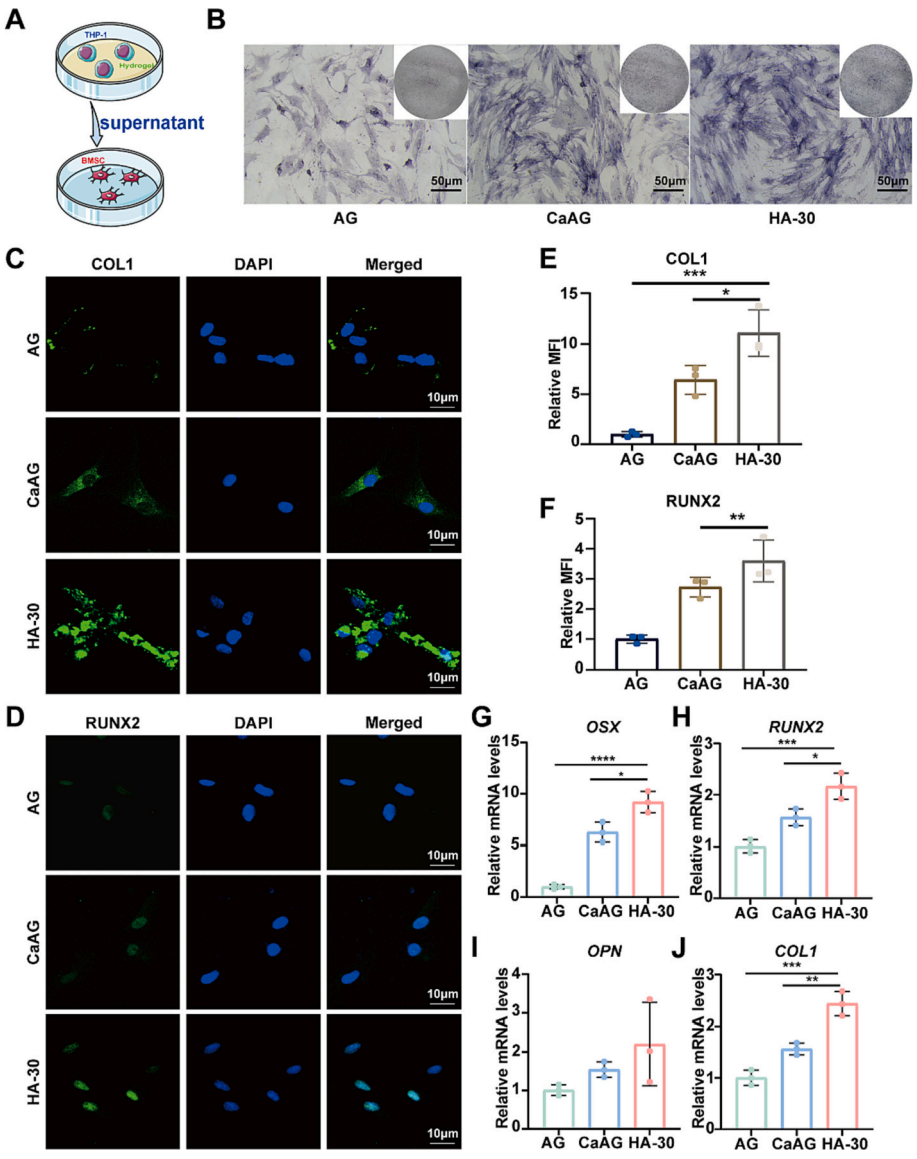

Fig. 5. nHA@Gel/ADA induced h-BMSCs osteogenic differentiation via macrophage M2 polarization. A) Schematic illustration of the process that THP-1 cells cultured on composite hydrogels induced h-BMSCs osteogenic differentiation. B) The ALP staining results after 7 days (scale bar = 50 μm). C and D) Immunostaining of osteo-related markers expressed by h-BMSCs under different conditions on day 7. COL1 (green), RUNX2 (green), and DAPI (blue) (scale bar = 10 μm). E and F) Relative mean fluorescence intensity analysis of COL1 and RUNX2 by ImageJ software. G, H, I, J) The expression of osteo-related genes including *OSX*, *RUNX2*, *OPN* and *COL1*. $^{*}p < 0.05$, $^{**}p < 0.01$, $^{***}p < 0.001$ and $^{****}p < 0.0001$.

That might be ascribed to the landscape of hydrogel surface discussed above, as the sizes of evenly distributed poles on the surface of composite hydrogels match up with both of the diameters of macrophages and BMSCs, suitable for functional activation and signal transduction for the two types of cells. Thus, the novel surface morphological variations induced by addition of nHA displayed its universality in regulation of cellular behaviors.

3.7. nHA@ADA-Gel facilitated in vivo bone regeneration

To verify the role of nHA@ADA-Gel in the induction of new bone formation, we assessed the in vivo bone regeneration potential of composite hydrogels using the SD rat cranial defect model (Fig. S17). Photographs and H&E staining results of bone defect restoration under different treatments revealed that skull defects in HA-30 group were almost covered by newly created bone tissue compared to those in AG and CaAG groups (Fig. 6A–B). Masson staining results observed a predominantly accelerated deposition of type 1 collagen in repaired regions (Fig. S18). Meanwhile, immunofluorescence assays revealed that COL1 and RUNX2, two indicators of osteogenesis, displayed significantly increased expression levels in newly formed bone tissues in HA-30 group (Fig. 6C–D). Besides, increased infiltration of M2 like macrophages into repairing sites was also detected by confocal microscopy (Fig. 6E), suggesting the role of HA-30 in induction of macrophage M2 polarization. The skull defect samples were harvested 6 weeks after the operation, followed by the measurement using micro-CT. As illustrated below, the quality and quantity of newly formed bone tissues in HA-30 group were much higher compared with the other two groups (Fig. 6F–J) ($p < 0.0001$). Altogether, these results indicated that HA-30 acted well as a bioactive candidate for in vivo bone regeneration. When combined with the in vitro results, they altogether demonstrated that nHA@ADA-Gel could accelerate new bone formation by offering a platform for mutual regulation of macrophages and BMSCs. Previous studies have observed direct osteogenic effect of different types of nHA-loaded biomaterials, biological functions of which were mainly attributed to nHA itself and slow release of Ca^{2+} (Zhong et al., 2022). Here, we observed a special morphological remodeling on the surface of hydrogels upon decoration of nHA, which worked as a bioactive interactive platform for effective bone repair through macrophage/mesenchymal stem cell crosstalk(Xiangji et al., 2021).

4. Conclusion

In this work, we have demonstrated the simultaneous enhancement

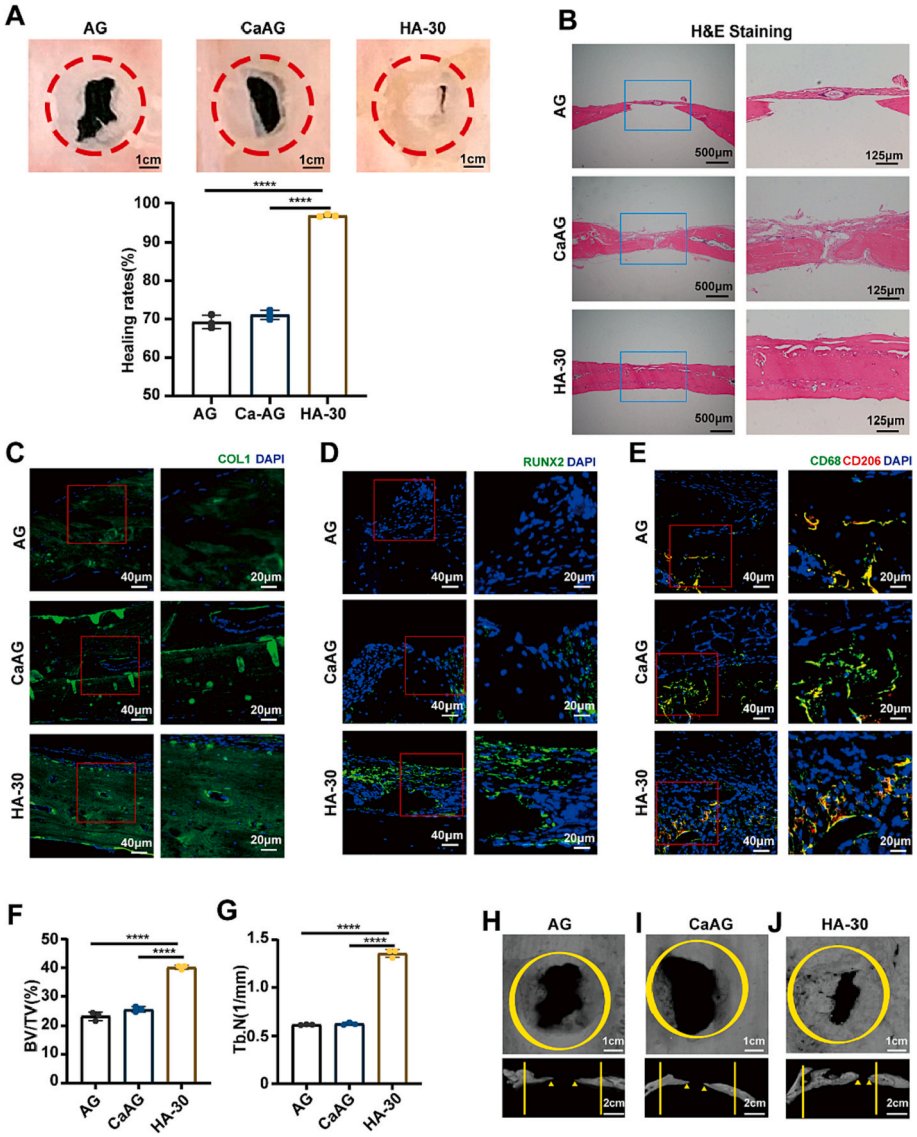

Fig. 6. nHA@Gel/ADA promoted bone regeneration in vivo.
A) The images of calvarial bone specimens. Red circles denote the boundary between new bone and host bone. B) The H&E staining of cranial bone specimens (scale bars = 500 μm and 125 μm). C, D and E) Immunofluorescence staining of COL1 (green), RUNX2 (green) and CD68+ (green) CD206+ (red) macrophages in the repaired defect area (scale bars = 40 μm and 20 μm). F and G) Morphometric analysis of bone volume/total volume (BV/TV) and trabeculae number (Tb.N). $^{*}p < 0.05$, $^{**}p < 0.01$, $^{***}p < 0.001$ and $^{****}p < 0.0001$. H, I and J) Representative CT images of bone regeneration within calvarial bone defects at 6 weeks after injection of composite hydrogels. Yellow triangles denote nascent bone. Yellow circles denote the boundary between new bone and host bone.

of physical features and bioactive effect in a novel nHA@ADA-Gel. The double cross-linking strategy endows the hydrogel with excellent injectability, self-healing property and shape adaptability, which are necessary for repair of irregular facial bone defects. Decoration of nHA helps the hydrogel not only achieve strengthened mechanical properties, but also promotes the remodeling of surface appearance to a size-confined poly-porous surface, suitable for efficient crosstalk between macrophages and BMSCs and subsequent osteogenesis. The nHA@ADA-Gel proposed here successfully integrated inherent features and bioactive functions for osteogenesis, therefore offering promising opportunities toward developing new biomaterials specifically applied in repair of maxillofacial bone defects.

CRediT authorship contribution statement

Jiwei Sun, Haojie Wei: Conceptualization, Methodology, Software Xiaohu Zhou, Keqi Wo.: Data curation, Writing- original draft preparation. Haoqi Lei, Junyuan Zhang, Xiaofeng Lu, Feng Mei: Visualization, Investigation. Qingming Tang, Yifan Wang, Zhiqiang Luo, Lihong Fan: Software, Validation. Yingying Chu, Lili Chen: Supervision, Writing-reviewing and editing.

Declaration of competing interest

The authors declare no conflicts of interests for this article.

Data availability

No data was used for the research described in the article.

Appendix A. Supplementary data

Supplementary data to this article can be found online at https://doi.org/10.1016/j.carbpol.2022.120127.

References

Bai, X., Lü, S., Liu, H., Cao, Z., Ning, P., Wang, Z., & Liu, M. (2017). Polysaccharides based injectable hydrogel compositing bio-glass for cranial bone repair. *Carbohydrate Polymers, 175*, 557–564.

Barros, J., Ferraz, M. P., Azeredo, J., Fernandes, M. H., Gomes, P. S., & Monteiro, F. J. (2019). Alginate-nanohydroxyapatite hydrogel system: Optimizing the formulation for enhanced bone regeneration. *Materials Science and Engineering: C, 105*, Article 109985.

Belema-Bedada, F., Uchida, S., Martire, A., Kostin, S., & Braun, T. (2008). Efficient homing of multipotent adult mesenchymal stem cells depends on FROUNT-mediated clustering of CCR2. *Cell Stem Cell, 2*(6), 566–575.

Chen, L., Tredget, E. E., Wu, P. Y., & Wu, Y. (2008). Paracrine factors of mesenchymal stem cells recruit macrophages and endothelial lineage cells and enhance wound healing. *PLoS One, 3*(4), Article e1886.
Chen, Z., Tang, J., Zhang, N., Chen, Y., Chen, Y., Li, H., & Liu, H. (2022). Dual-network sodium alginate/polyacrylamide/laponite nanocomposite hydrogels with high toughness and cyclic mechano-responsiveness. *Colloids and Surfaces A: Physicochemical and Engineering Aspects, 633*, Article 127867.
Ding, W., Zhou, J., Zeng, Y., Wang, Y.-N., & Shi, B. (2017). Preparation of oxidized sodium alginate with different molecular weights and its application for crosslinking collagen fiber. *Carbohydrate Polymers, 157*, 1650–1656.
Elsalanty, M. E., & Genecov, D. G. (2009). Bone grafts in craniofacial surgery. *Craniomaxillofacial Trauma & Reconstruction, 2*(3), 125–134.
Emami, Z., Ehsani, M., Zandi, M., & Foudazi, R. (2018). Controlling alginate oxidation conditions for making alginate-gelatin hydrogels. *Carbohydrate Polymers, 198*, 509–517.
Evans, N. D., Oreffo, R. O. C., Healy, E., Thurner, P. J., & Man, Y. H. (2013). Epithelial mechanobiology, skin wound healing, and the stem cell niche. *Journal of the Mechanical Behavior of Biomedical Materials, 28*, 397–409.
Giovanna, C., Salvatore, P., Domenico, F., Giuseppe, N., Claudia, F., Lucia, F., & Sabrina, C. (2020). A new Ag-nanostructured hydroxyapatite porous scaffold: Antibacterial effect and cytotoxicity study. *Materials Science and Engineering: C, 118*, Article 111394.
Graham, G. W., Ryan, C. R., Elizabeth, R. Z., Tripp, L., John, S. F., Michael, S. H., & Derrick, C. W. (2016). Stem cells in bone regeneration. *Stem Cell Reviews and Reports, 12*(5), 524–529.
Hassani, A., Khoshfetrat, A. B., Rahbarghazi, R., & Sakai, S. (2022). Collagen and nano-hydroxyapatite interactions in alginate-based microcapsule provide an appropriate osteogenic microenvironment for modular bone tissue formation. *Carbohydrate Polymers, 277*, Article 118807.
Hongbo, Z., Min, L., Yajie, Z., Jingbo, Y., & Renjun, P. (2020). Nanocomposite hydrogels for tissue engineering applications. *Nanoscale, 12*(28), 14976–14995.
Huang, Y., Mu, L., Zhao, X., Han, Y., & Guo, B. (2022). Bacterial growth-induced tobramycin smart release self-healing hydrogel for Pseudomonas aeruginosa-infected burn wound healing. *ACS Nano, 16*(8), 13022–13036.
Hurle, K., Maia, F. R., Ribeiro, V. P., Pina, S., Oliveira, J. M., Goetz-Neunhoeffer, F., & Reis, R. L. (2022). Osteogenic lithium-doped brushite cements for bone regeneration. *Bioactive Materials, 16*, 403–417.
Jejurikar, A., Seow, X. T., Lawrie, G., Martin, D., Jayakrishnan, A., & Grondahl, L. (2012). Degradable alginate hydrogels crosslinked by the macromolecular crosslinker alginate dialdehyde. *Journal of Materials Chemistry, 22*(19), 9751–9758.
Jin, S.-S., He, D.-Q., Luo, D., Wang, Y., Yu, M., Guan, B., & Liu, Y. (2019). A biomimetic hierarchical nanointerface orchestrates macrophage polarization and mesenchymal stem cell recruitment to promote endogenous bone regeneration. *ACS Nano, 13*(6), 6581–6595.
Krombach, F., Münzing, S., Allmeling, A. M., Gerlach, J. T., Behr, J., & Dörger, M. (1997). Cell size of alveolar macrophages: an interspecies comparison. *Environmental Health Perspectives, 105*(5), 1261–1263.
Li, Z., Chen, X., Bao, C., Liu, C., Liu, C., Li, D., & Lin, Q. (2021). Fabrication and evaluation of alginate/bacterial cellulose nanocrystals–chitosan–gelatin composite scaffolds. *Molecules, 26*(16), 5003.
Lloyd, A. C. (2013). The regulation of cell size. *Cell, 154*(6), 1194–1205.
Ma, D., E, T., & Yang, S. (2021). Efficient removal of Cu(II) with graphene oxide-titanium dioxide/sodium alginate composite beads: Preparation, characterization, and adsorption mechanism. *Journal of Environmental Chemical Engineering, 9*(6), Article 106501.
Maggini, J., Mirkin, G., Bognanni, I., Holmberg, J., Piazzón, I. M., Nepomnaschy, I., & Geffner, J. R. (2010). Mouse bone marrow-derived mesenchymal stromal cells turn activated macrophages into a regulatory-like profile. *PLoS One, 5*(2), Article e9252.
Mueller, R. L. (2015). 基因组生物学和细胞大小多样性的进化. *Cold Spring Harbor Perspectives in Biology, 7*, a019125.
Murray, P. J., & Wynn, T. A. (2011). Protective and pathogenic functions of macrophage subsets. *Nature Reviews Immunology, 11*(11), 723–737.
Rumpler, M., Woesz, A., Dunlop, J. W. C., van Dongen, J. T., & Fratzl, P. (2008). The effect of geometry on three-dimensional tissue growth. *Journal of the Royal Society Interface, 5*(27), 1173–1180.
Samsonraj, R. M., Raghunath, M., Nurcombe, V., Hui, J. H., van Wijnen, A. J., & Cool, S. M. (2017). Concise review: Multifaceted characterization of human mesenchymal stem cells for use in regenerative medicine. *Stem Cells Translational Medicine, 6*(12), 2173–2185.
Short, A. R., Koralla, D., Deshmukh, A., Wissel, B., Stocker, B., Calhoun, M., & Winter, J. O. (2015). Hydrogels that allow and facilitate bone repair, remodeling, and regeneration. *Journal of Materials Chemistry B, 3*(40), 7818–7830.
Sylwia, D., Anna, A., Miroslaw, J., & Barbara, L. (2020). Immunomodulatory and regenerative effects of mesenchymal stem cells and extracellular vesicles: Therapeutic outlook for inflammatory and degenerative diseases. *Frontiers in Immunology, 11*, Article 591065.
Tan, B., Tang, Q., Zhong, Y., Wei, Y., He, L., Wu, Y., & Liao, J. (2021). Biomaterial-based strategies for maxillofacial tumour therapy and bone defect regeneration. *International Journal of Oral Science, 13*(1), 9.
Wang, Y., Wang, J., Gao, R., Liu, X., Feng, Z., Zhang, C., & Wang, W. (2022). Biomimetic glycopeptide hydrogel coated PCL/nHA scaffold for enhanced cranial bone regeneration via macrophage M2 polarization-induced osteo-immunomodulation. *Biomaterials, 285*, Article 121538.
Xiangji, L., Yihang, M., Minjiang, C., Jiansong, J., Yuhang, Z., Qingsan, Z., & Peibiao, Z. (2021). Ba/Mg co-doped hydroxyapatite/PLGA composites enhance X-ray imaging and bone defect regeneration. *Journal of Materials Chemistry B, 9*(33), 6691–6702.
Yin, L., Hongbing, D., Chunlian, X., Chengfeng, X., & Xue, Z. (2014). Cytotoxicity of calcium rectorite micro/nanoparticles before and after organic modification. *Chemical Research in Toxicology, 27*(8), 1401–1410.
Yinghua, X., Elizabeth, A. F., Stevin, H. G., & Michael, S. D. (2013). Mechanical testing of hydrogels in cartilage tissue engineering: Beyond the compressive modulus. *Tissue Engineering, Part B: Reviews, 19*(5), 403–412.
Zheng, Y., Han, Q., Wang, J., Li, D., Song, Z., & Yu, J. (2020). Promotion of osseointegration between implant and bone interface by titanium alloy porous scaffolds prepared by 3D printing. *ACS Biomaterials Science & Engineering, 6*(9), 5181–5190.
Zhong, Z., Wu, X., Wang, Y., Li, M., Li, Y., Liu, X., & Zhang, S. (2022). Zn/Sr dual ions-collagen co-assembly hydroxyapatite enhances bone regeneration through procedural osteo-immunomodulation and osteogenesis. *Bioactive Materials, 10*, 195–206.
Zhu, Y., Liang, H., Liu, X., Wu, J., Yang, C., Wong, T. M., & Yeung, K. W. K. (2021). Regulation of macrophage polarization through surface topography design to facilitate implant-to-bone osteointegration. *Science Advances, 7*(14), Article eabf6654.